

Snell’s Law for Swimmers

Tyler D. Ross^{1,*}, Dino Osmanović², John F. Brady³, and Paul W. K. Rothmund¹

¹Department of Computing and Mathematical Sciences, California Institute of Technology, Pasadena, CA 91125, USA.

²Center for the Physics of Living Systems, Department of Physics, Massachusetts Institute of Technology, Cambridge, Massachusetts 02139, USA

³Divisions of Chemistry & Chemical Engineering and Engineering & Applied Science, California Institute of Technology, Pasadena, CA 91125, USA

*correspondence to: tross@caltech.edu

Snell’s law, which encompasses both refraction and total internal reflection, provides the foundation for ray optics and all lens-based instruments, from microscopes to telescopes. Refraction results when light crosses the interface between media of different refractive index, the dimensionless number that captures how much a medium retards the propagation of light. In this work, we show that the motion of self-propelled particles moving across a drag discontinuity is governed by an analogous Snell’s law, allowing for swimmer ray optics. We derive a variant of Snell’s law for swimmers moving across media of different viscosities. Just as the ratio of refractive indexes sets the path of a light ray, the ratio of viscosities is shown to determine the trajectories of swimmers. We find that the magnitude of refraction depends on the swimmer’s shape, specifically the aspect ratio, as analogous to the wavelength of light. This enables the demixing of a polymorphic, many-shaped, beam of swimmers into distinct monomorphic, single-shaped, beams through a viscosity prism. In turn, beams of monomorphic swimmers can be focused by spherical and gradient viscosity lenses. Completing the analogy, we show that the shape-dependence of the total internal reflection critical angle can be used to create swimmer traps. Such analogies to ray optics suggest a universe of new devices for sorting, concentrating, and analyzing microscopic swimmers is possible.

Introduction

Directed transport of matter on the microscale is a fundamental process in biology [1–3], lab-on-a-chip systems [4, 5], and drug delivery [6–8]. One of the primary modes of directed transport relies on the dynamics of micro-swimmers, or self-propelled particles. A substantial body of work has demonstrated that swimmer density can be spatially modulated using asymmetric barriers [9, 10], differing regions of propulsion speed [11–14], run-and-tumble dynamics [15], motility induced phase separation [16], and dynamic swimmer affinities [17]. However, there are few known mechanisms for controlling the trajectories of swimmers. Recently, there has been evidence that swimmers refract and scatter at drag discontinuities [18–20]. While there is theory that studies the movement of spherical swimmers down viscosity gradients [21] and theory that predicts that nonuniaxial

swimmers can swim up viscosity gradients [22], there is no theory for swimmers encountering drag discontinuities. Here we derive a Snell’s law for swimmers, which predicts how a swimmer’s trajectory is changed when traversing a viscosity discontinuity and can be used to rationally design optics-like devices for swimmers.

Derivation

We consider the trajectory of a swimmer moving across a drag discontinuity at low Reynold’s number; for simplicity, we ignore hydrodynamic and Brownian interactions and assume that the interface at the discontinuity does not deform as the swimmer passes through.

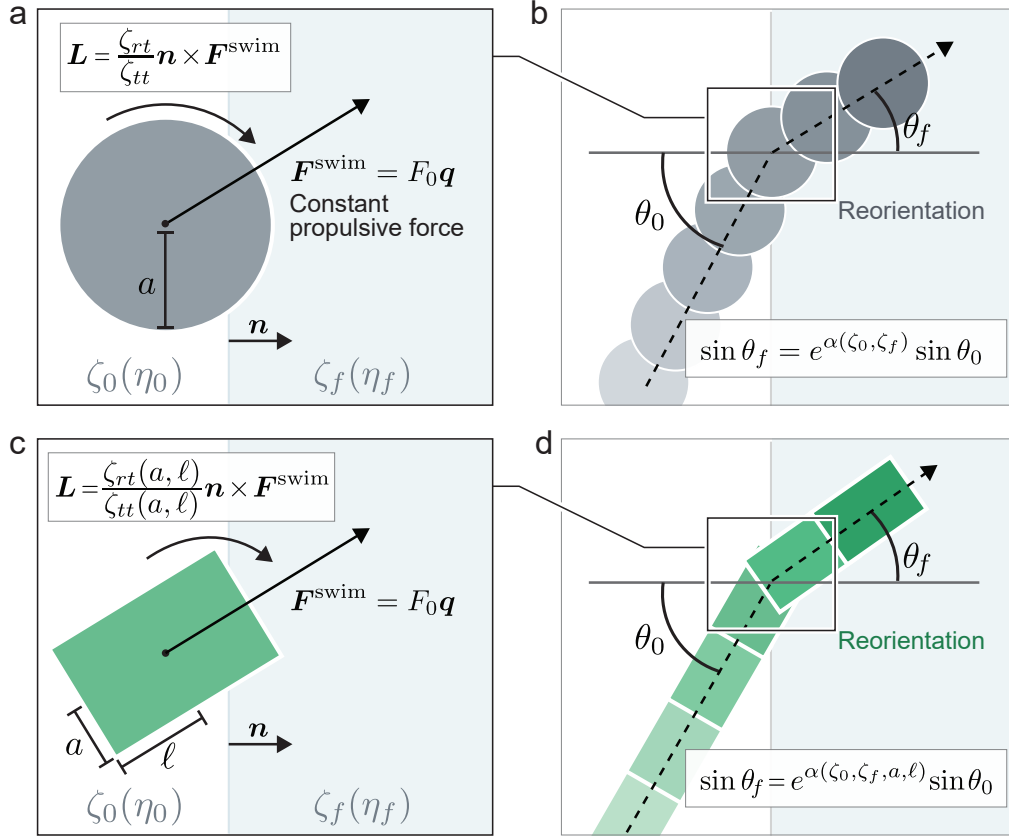


Figure 1: Sketch of spherical and rectangular swimmers moving across a drag (e.g. viscosity or resistivity) discontinuity. **a**, Depiction of the relevant forces and torques on a swimmer as it travels across a drag discontinuity. **b**, The forces and torques from **(a)** cause a reorientation of the swimmer’s trajectory around the drag discontinuity. **c**, **d**, Forces and re-orientation of a rectangular swimmer depend on the aspect ratio of the swimmer.

As illustrated in Fig. 1, the non-accelerating motion of the swimmer follows from a balance between the drag force, $\mathbf{F}^{drag} = -\mathbf{R}_{FU} \cdot \mathbf{U}$, and a propulsive or swim force, \mathbf{F}^{swim} :

$$0 = -\mathbf{R}_{FU} \cdot \mathbf{U} + \mathbf{F}^{swim}. \quad (1)$$

In Eq. (1), \mathbf{U} is the translational velocity of the swimmer, and \mathbf{R}_{FU} is the (hydrodynamic) resistance function that gives the coupling between the drag and the velocity. The resistance tensor depends

on the jump in resistivity, and the geometry—the size and shape of the swimmer as well as its proximity and orientation relative to the discontinuity.

A swimmer is an active particle, pushing off its surroundings and generating a propulsive swim force of the form: $\mathbf{F}^{swim} = F_0 \mathbf{q}$, where F_0 is the magnitude and \mathbf{q} the direction of propulsion. To simplify the analysis, we take the resistance tensor to be isotropic and constant, $\mathbf{R}_{FU} = \zeta_{tt} \mathbf{I}$, where ζ_{tt} is the translational drag coefficient and \mathbf{I} is the identity tensor. Thus, the velocity is

$$\mathbf{U} = F_0 \mathbf{q} / \zeta_{tt}. \quad (2)$$

We consider a constant magnitude swim force F_0 and thus the speed of the swimmer is slower in the region of greater resistivity (or greater viscosity). For example, for a spherical swimmer in a Newtonian fluid of viscosity η we have the well-known Stokes drag coefficient $\zeta_{tt} = 6\pi\eta a$, where a is the swimmer radius.

The swimming direction \mathbf{q} changes as a function of time according to

$$\frac{d\mathbf{q}}{dt} = \boldsymbol{\Omega} \times \mathbf{q}, \quad (3)$$

where $\boldsymbol{\Omega}$ is the angular velocity of the swimmer. The swimmer angular velocity follows from the torque balance for the force- and torque-free motion

$$0 = -\mathbf{R}_{L\Omega} \cdot \boldsymbol{\Omega} - \mathbf{R}_{LU} \cdot \mathbf{U}. \quad (4)$$

In Eq. (4) $\mathbf{R}_{L\Omega}$ is the resistance tensor coupling the torque (\mathbf{L}) to the angular velocity, and \mathbf{R}_{LU} couples the torque to the translational velocity. As for the force-velocity coupling (FU), we take the torque-angular velocity coupling to be isotropic and constant: $\mathbf{R}_{L\Omega} = \zeta_{rr} \mathbf{I}$; for a spherical swimmer in a viscous fluid $\zeta_{rr} = 8\pi\eta a^3$.

The torque-translational velocity (LU) coupling arises because as the swimmer crosses into a region of higher resistivity that portion of the swimmer in the more resistive medium slows down and thus the swimmer rotates such that its direction of motion tends to align along the normal as illustrated in Fig. 1a. The opposite occurs when moving into a less resistive medium. The LU coupling is a pseudo tensor and since the swimmer itself is not chiral, it must be of the form $\mathbf{R}_{LU} = \zeta_{rt} \boldsymbol{\epsilon} \cdot \mathbf{n}$, where $\boldsymbol{\epsilon}$ is the unit alternating tensor, \mathbf{n} is the normal to the discontinuity, and ζ_{rt} is the drag coefficient. For a sphere, the LU coupling only arises if there is a jump in resistivity, $\zeta_{rt} \sim 6\pi\Delta\eta a^2$.

Combining Eqs. (1) and (4), Eq. (3) becomes

$$\frac{d\mathbf{q}}{dt} = \frac{\zeta_{rt} F_0}{\zeta_{rr} \zeta_{tt}} (\mathbf{n} \times \mathbf{q}) \times \mathbf{q} = \frac{\zeta_{rt} F_0}{\zeta_{rr} \zeta_{tt}} [\mathbf{n} - \mathbf{q}(\mathbf{q} \cdot \mathbf{n})]. \quad (5)$$

Now, $\mathbf{n} \cdot \mathbf{q} = \cos\theta$, where θ is the angle between the normal and the swim direction, and thus Eq. (5) gives an equation for the evolution of $\theta(t)$:

$$\frac{d \cos \theta}{\sin^2 \theta} = \frac{\zeta_{rt} F_0}{\zeta_{rr} \zeta_{tt}} dt. \quad (6)$$

We need to integrate Eq. (6) from the time the swimmer first touches the discontinuity ($t = 0$) with incident angle θ_0 until it fully crosses into the next region at the final time t_f , which will then give the out-going angle θ_f . The time to cross the interface follows from the translational velocity

$d\mathbf{x}/dt = \mathbf{U}$, and since only the normal component of the velocity is responsible for the swimmer crossing we have

$$\frac{d(\mathbf{n} \cdot \mathbf{x})}{dt} = \frac{F_0}{\zeta_{tt}} \mathbf{n} \cdot \mathbf{q} = \frac{F_0}{\zeta_{tt}} \cos \theta. \quad (7)$$

We can use Eq. (7) to replace dt in Eq. (6) to give

$$dx_{\perp} = \frac{\zeta_{rr} \cos \theta d \cos \theta}{\zeta_{rt} \sin^2 \theta} = -\frac{\zeta_{rr}}{\zeta_{rt}} d \ln(\sin \theta), \quad (8)$$

where $x_{\perp} = \mathbf{n} \cdot \mathbf{x}$ is the amount of the swimmer that has crossed the interface. For a spherical swimmer, integrating from 0 to $2a$ relates the initial to the final angle and yields a Snell's law:

$$\sin \theta_f = e^{\alpha} \sin \theta_0, \quad (9)$$

where $\alpha = -2a\zeta_{rt}/\zeta_{rr}$. This behavior is independent of the magnitude of the propulsive force F_0 and the Stokes drag ζ_{tt} . Further by dimensional arguments, the drag coefficient for LU coupling is proportional to a^2 and thus α is also independent of the size of the swimmer. The validity of this Snell's law and its independence on the swimmer size are verified by direct simulation below.

We have made a number of approximations in arriving at this Snell's law. First, we have assumed that the drag coefficients ζ_{rr} and ζ_{rt} are constants (Note that ζ_{tt} cancels out in Eq. (8)). Both are proportional to the local value of the resistance or viscosity of the medium and thus depend on the portion of the swimmer in each region. We can include this effect by noting that Eq. (8) can be written as

$$\frac{\zeta_{rt}(x_{\perp})}{\zeta_{rr}(x_{\perp})} dx_{\perp} = -d \ln(\sin \theta), \quad (10)$$

and integration from 0 to $2a$ again recovers Snell's law Eq. (9) where α is now given by

$$\alpha = - \int_0^{2a} \frac{\zeta_{rt}(x_{\perp})}{\zeta_{rr}(x_{\perp})} dx_{\perp}. \quad (11)$$

From a micromechanical model for $\zeta_{rr}(x_{\perp})$ and $\zeta_{rt}(x_{\perp})$ one could compute α ; the result will be the form

$$\alpha = -C \frac{\Delta\eta}{\langle\eta\rangle}, \quad (12)$$

where $\Delta\eta = \eta_f - \eta_0$, $\langle\eta\rangle = (\eta_f + \eta_0)/2$ and C is an order 1 constant that is (weakly) dependent of the viscosity ratio η_f/η_0 (Fig. 1b). Later we show that Snell's law with Eq. (12) is in excellent agreement with detailed micromechanical simulations.

Since the reorientation arises because part of the swimmer finds itself in a more resistive medium, if the swimmer is very thin relative to its swim axis, then the differential resistance across the body is small and the reorientation should be reduced. An infinitely thin swimmer will not reorient at all. We can account for this shape effect in a simple manner by recognizing that the amount of the swimmer that has crossed the discontinuity Δx_{\perp} depends on the body shape and the initial orientation θ_0 . For a simple rectangular swimmer shown in Fig. 1c,d,

$$\Delta x_{\perp} = \ell \cos \theta_0 + a(1 - \cos \theta_0), \quad (13)$$

where ℓ is the half major length and a is the half minor length. Using this in Eq. (8) we again have Snell's law, but now

$$\alpha \sim -\frac{a}{\ell^2} (a + (\ell - a) \cos \theta_0) \frac{\Delta\eta}{\langle\eta\rangle}, \quad (14)$$

where we have used the geometric scaling that $\zeta_{rt}/\zeta_{rr} \sim a/\ell^2$. We have also assumed the instantaneous orientation angle of the body could be approximated with its initial angle θ_0 . When $\ell = a$, Eq. (14) reduces to Eq. (12). The dependence on the aspect ratio is similar to the wavelength dependence of the refractive index. We later use numerical simulations to test this prediction.

We mention a few caveats. Above we assumed that any force-angular velocity coupling $\mathbf{R}_{F\Omega} = \mathbf{R}_{LU}^\dagger$ was negligible. If $\mathbf{R}_{F\Omega}$ is included, the force balance Eq. (1) now becomes $0 = -\mathbf{R}_{FU} \cdot \mathbf{U} - \mathbf{R}_{F\Omega} \cdot \boldsymbol{\Omega} + \mathbf{F}^{swim}$, and, when combined with the angular momentum balance Eq. (4), will give an angular velocity $\boldsymbol{\Omega} = -\mathbf{R}_{L\Omega}^{-1} \cdot \mathbf{R}_{LU} \cdot [\mathbf{R}_{FU} - \mathbf{R}_{F\Omega} \cdot \mathbf{R}_{L\Omega}^{-1} \cdot \mathbf{R}_{LU}]^{-1} \cdot \mathbf{F}^{swim}$. The additional factor $\mathbf{R}_{F\Omega} \cdot \mathbf{R}_{L\Omega}^{-1} \cdot \mathbf{R}_{LU}$ will now add an additional θ dependence to Eq. (6) and we can only derive a Snell's law under the condition that $\zeta_{rt}^2/(\zeta_{rr}\zeta_{tt}) \ll 1$. Furthermore non-spherical swimmers will not, in general, have isotropic resistance tensors and we can expect, e.g., the force-velocity coupling to have the form $\mathbf{R}_{FU} = \zeta_{\parallel} \mathbf{q}\mathbf{q} + \zeta_{\perp} (\mathbf{I} - \mathbf{q}\mathbf{q})$, where ζ_{\parallel} and ζ_{\perp} are drag coefficients for motion parallel and perpendicular to the swimmer axis, which we assume be the same as the direction of propulsion \mathbf{q} . There will also be similar forms for $\mathbf{R}_{L\Omega}$ and \mathbf{R}_{LU} . Clearly, this complicates the analysis and in general it may be impossible to find a Snell-like analytical expression for the refraction of nonspherical swimmers.

Finally, our neglect of hydrodynamic interactions enables us to assume that there is no interaction between the swimmer and the drag discontinuity until they make physical contact. In general, the introduction of hydrodynamic interactions will make resistance tensors depend on the distance of the swimmer from the discontinuity. The magnitude of such effects will depend on the swimmer type—pusher, puller, or neutral—and the magnitude of the discontinuity. Neutral swimmers, with their more uniform flow fields, might be expected to give refraction similar to that predicted here, but in general but it is unlikely that simple Snell's law will emerge once hydrodynamics is considered. Two observations are worth making. First, the force- and torque-balance approach taken here will apply and contribute terms to any full hydrodynamic treatment which seeks to calculate the refraction of a swimmer moving through a drag discontinuity. Second, for crawlers [23] whose propulsive force is generated by interaction with a surface rather than a fluid, the Snell's law derived here may apply with little or no modification.

Analysis of results

Simulations of the spherical swimmer closely agree with Eqs. (9) and (12) (Fig. 2a, see Methods and Supplementary Information for detail of simulation and curve fitting; see [Video 1](#) for an example simulation). One prediction from our theory is that refraction is size independent. By simulating swimmers of different sizes, we find that the angle of refraction is indeed size invariant (Fig. S2a). Further, the form of our Snell's law for a spherical swimmer implies that there is a symmetry about the line $\theta_f = \theta_0$. We are able to verify this prediction by comparing the data points and curves across this axis of symmetry (Fig. S2b).

As for Snell's law, when $\eta_f/\eta_0 < 1$, Eq. (9) is valid up to $\theta_f = \frac{\pi}{2}$. For $\theta_f = \frac{\pi}{2}$, the incident critical angle is

$$\theta_{\text{crit}} = \arcsin e^{-\alpha}. \quad (15)$$

For $\theta_0 > \theta_{\text{crit}}$ swimmers obey the law of reflection,

$$\theta_f = \pi - \theta_0, \quad (16)$$

which we confirm with simulations (Fig. 2b). Through symmetry, the critical angle is the same as Snell's window, which is the greatest possible refraction angle for a given $\eta_f/\eta_0 > 1$.

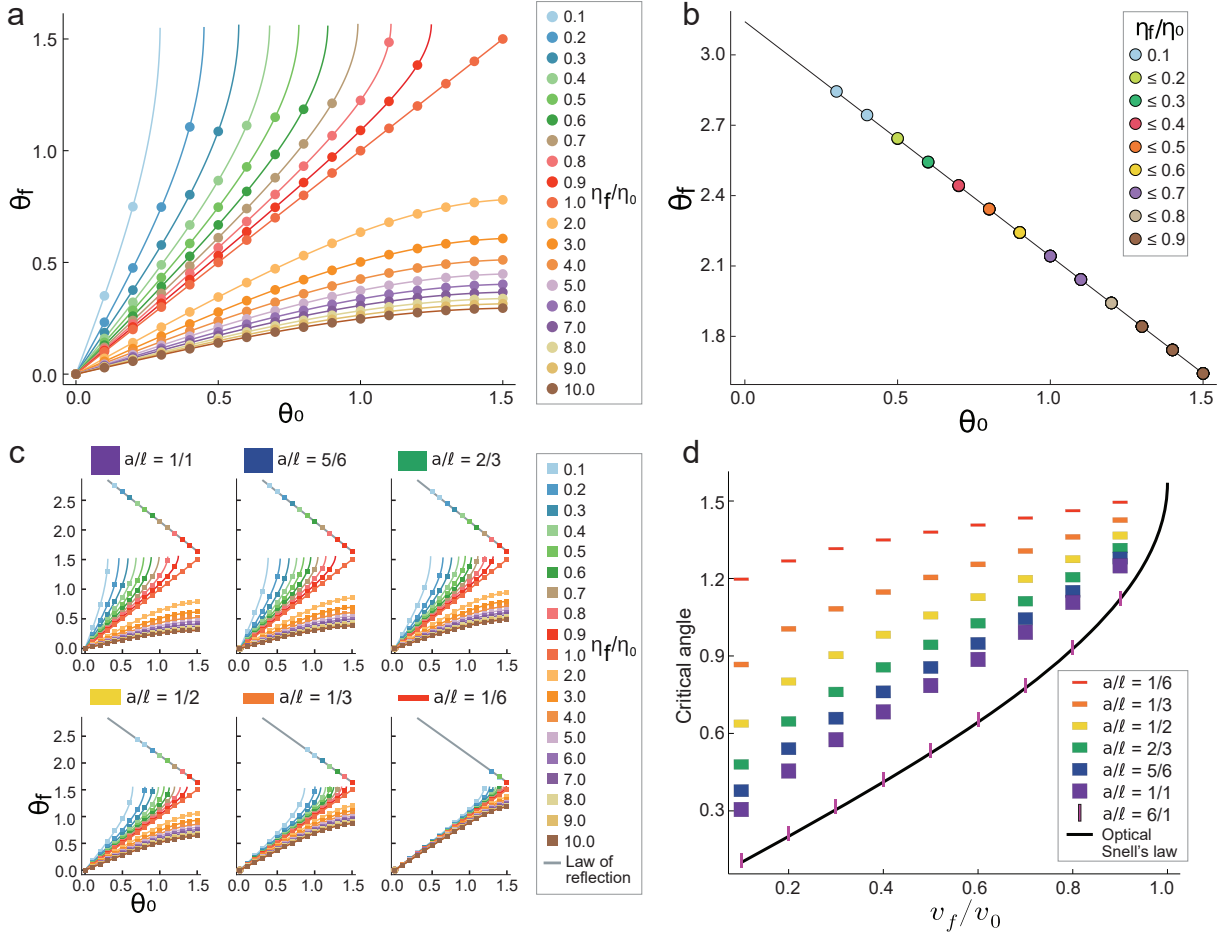


Figure 2: Swimmers refract and reflect in a manner analogous to Snell's law. **a**, Spherical swimmer refraction as a function of incident angle and viscosity ratios. Curves represent theory, points represent simulations. **b**, For incident angles above the critical angle, swimmers follow the law of reflection as indicated by the black line. Note that points overlap each other, as indicated in the legend. **c**, Refraction and reflection for rectangular swimmers of varying thicknesses. Note that points on the law of reflection line overlap each other in the same order as (b). **d**, Comparison between the critical angles predicted by optical Snell's law and swimmer Snell's law.

For the rectangular swimmer, we see that refraction depends on the swimmer's aspect ratio in Eq. (14). As the swimmer's aspect ratio becomes smaller relative to its swim axis, the effect of refraction diminishes (Fig. 2c). In the limit that the swimmer becomes a 1D-line along the swim axis, i.e. $a = 0$, the swimmer undergoes no refraction. In contrast, as the swimmer's aspect ratio becomes wider relative to its swim axis, there is a greater refraction effect.

Due to the similarities between our theory and optical Snell's law, we compare the two theories in more detail. The ratio of refractive indices can be rewritten as a ratio of speeds $\frac{n_f}{n_0} = \frac{c/v_f}{c/v_0} = \frac{v_f}{v_0}$, and we can similarly do this for the ratio of viscosities $\frac{\eta_f}{\eta_0} = \frac{F/v_f}{F/v_0} = \frac{v_f}{v_0}$. Thus, we can compare optical Snell's law, $v_f \sin \theta_f = v_0 \sin \theta_0$, to Eqs. (9) and (14) by looking at the critical angle as a function of the speed ratio (Fig. 2d). Overall, the critical angles share a similar scaling. Swimmers tend to refract less than light for the same speed ratio. However, for the wide swimmer $a/l = 6/1$, we find a critical angle and refraction curves (Fig. S3) that closely follow the optical Snell's law. Based on this finding, we conjecture that as $a/l \rightarrow \infty$, a rectangular swimmer will be subject to

the optical Snell's law. We note that the critical angle for spherical swimmers is nearly identical for $a/\ell = 1/1$ rectangular swimmers, and therefore is not plotted in Fig. 2d (compare Fig. S1a and Fig. S1b, purple dots).

Ray optics for swimmers

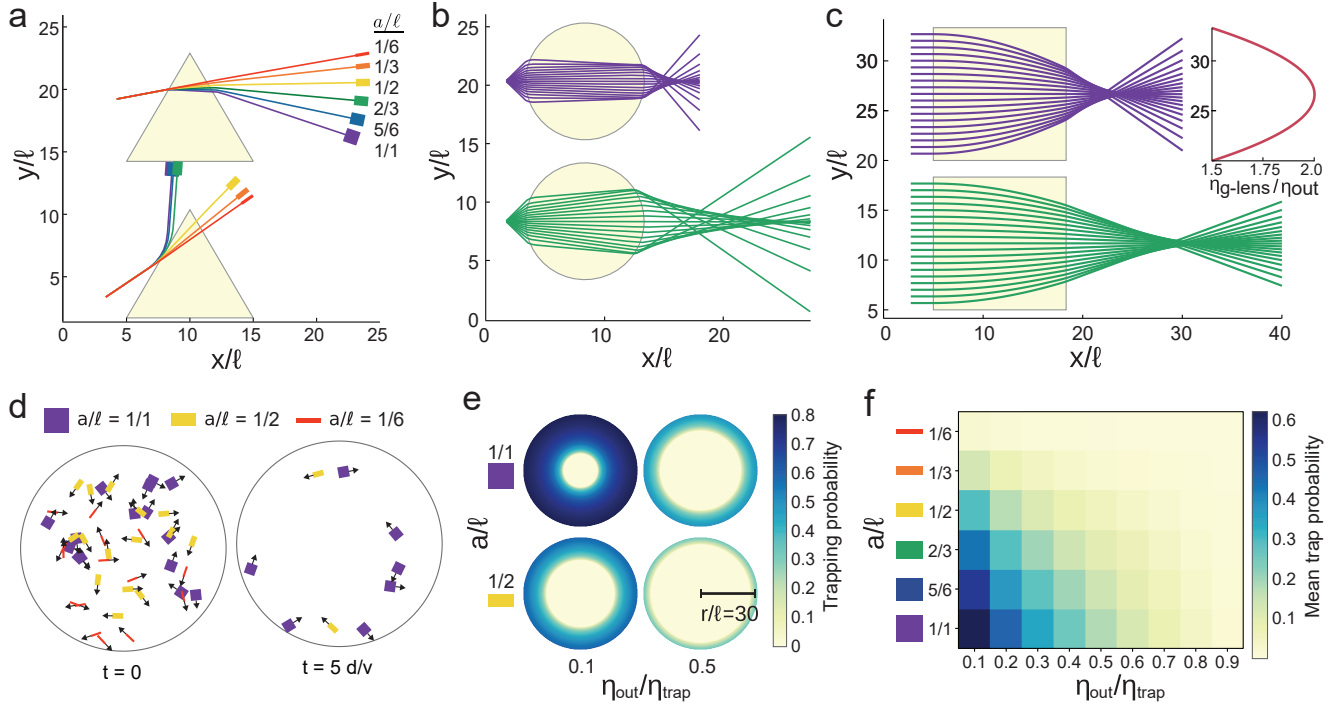


Figure 3: Principles of ray optics can be similarly applied to organize non-interacting swimmers. All results are from micromechanical simulations (see Sections S1.5 and S1.6). **a**, Prism analog disperses rectangular swimmers by their shape. Top: Swimmers disperse to different angles after passing through a region of higher viscosity ($\eta_{\text{prism}}/\eta_{\text{out}} = 2$). Bottom: A subset of swimmers reflect at a discontinuity of lower viscosity ($\eta_{\text{prism}}/\eta_{\text{out}} = 2/3$). **b**, Ball lens analog has different focal lengths and (spherical aberrations) depending on swimmer shape. Top: $a/\ell = 1$. Bottom: $a/\ell = 2/3$. **c**, Gradient lens analog focuses swimmers while reducing spherical aberrations. Top: $a/\ell = 1$, inset shows viscosity gradient of the lens. Bottom: $a/\ell = 2/3$. **d**, Frames of timelapse simulation for a swimmer trap. Time is measured in d/v where d is the trap diameter and v is the swimmer speed in the trap. **e**, Probability of a swimmer to be trapped given a random initial orientation at the indicated position. **f**, Mean trapping efficiency increases for smaller viscosity ratios and decreases for thinner swimmers.

The basis of ray optics is built on the refraction and reflection of light. Therefore, we consider if the principles of ray optics can also be applied to organize non-interacting swimmers. We start by creating a prism, where a triangular region has a viscosity that differs from the bulk solution (Fig. 3a)(Video 2). A polymorphic, multi-shaped, beam of swimmers is separated into monomorphic, single-shaped, beams by tuning the viscosity value of the triangular region. The results from our micromechanical simulations show a finite size effect not present for light. Although refraction and reflection angles are size independent, the centroid trajectory of a swimmer will appear to bend before encountering the interface (when the leading edge of the swimmer first contacts the interface)

and continue to bend beyond the interface (until the entire body of the swimmer is free from the discontinuity) as can be seen in Fig. S2a.

Having demonstrated that polymorphic beams of swimmers can be split into monomorphic beams, we investigate how these monomorphic beams can be shaped. A ball lens that draws swimmers toward a focal point can be created using a disk-shaped region with a higher viscosity than the bulk solution (Fig. 3b). The focus of the lens is a function of the viscosity ratio, the swimmer aspect ratio, and the size of the disk region. Like a ball lens for light, the ball lens for swimmers has spherical aberration, i.e. the trajectories of the swimmers do not all converge at a single focal point. In optics, aberrations are corrected by using compound lenses, aspheric lenses, or lenses with index gradients. We combine refraction with viscotaxis [21] to create a gradient viscosity lens (Fig. 3c) that can focus a collimated beam of monomorphic swimmers to a focal point with significantly reduced spherical aberration. Thus, beams of swimmers can be sculpted with lenses in a similar manner to light in optics.

While the principles of Snell’s law can be used to route swimmers in free space, they can also be used to confine swimmers. We trap swimmers in a disk with a higher viscosity than the bulk medium (Fig. 3d)([Video 3](#)). In this design, a swimmer with an incident angle greater than its critical angle will perpetually reflect off the boundary of the disk with the same incident angle. Swimmers whose orientation are below or equal to the critical angle, however, will pass through the trap. Consequently, the trap reaches its steady state by $t = d/v$, where d is the diameter of the disk and v is the swimmer speed inside the trap. The efficiency of the trap increases for smaller viscosity ratios (Fig. 3e,f). However, swimmers that are thin relative to their swim axis are trapped less effectively, such that a 1D swimmer cannot be trapped.

Conclusion

Our derivation of Snell’s law for swimmers is distinct from previous derivations of Snell’s law for light. In optics, Snell’s law has been derived based on the wave properties of light, or conservation of energy and momentum [24]. Such derivations are inaccessible here, as swimmers do not have wave-like properties, momentum is negligible at low Reynold’s number, and the energy of a self-propelled swimmer does not follow traditional energy conservation. (Note that previous work deriving an optimal navigation strategy for swimmers using Fermat’s principle results in a Snell’s law [25], but in doing so solves a problem that is unrelated to that treated here.) Instead, our derivation of Snell’s law for swimmers relies purely on mechanics, and comes from a transient, shape-dependent torque experienced by the swimmer during its short crossing of a drag discontinuity. To us it is surprising that such a local phenomena, so highly unrelated to light, can yield a theory of refraction so similar to that for light. Future work may expand the theory of Snell’s law for swimmers to include pusher- and puller-type swimmers, whose trajectory will be subject to hydrodynamic interactions with the drag discontinuity. It is also worth considering the physical or geometric properties of the swimmer, such as flexibility or chirality (e.g. left- or right- handed stars). These properties may allow for more exotic effects, such as a negative index of refraction.

There is little experimental data with any bearing on our Snell’s law; experiments for a few cell types show some form refraction or reflection when a swimmer encounters a drag discontinuity [18–20]. In once case [20], puller-type algal swimmers are observed to only reflect off of a boundary of low to high viscosity, which is the opposite of what our theory and simulation predicts. It is likely that this difference is a result of hydrodynamic interactions, which are not included in our theory. An experimental system of crawlers moving across a drag or friction discontinuity would have less pronounced hydrodynamic effects and therefore be better suited for directly testing our theory.

Our numerical simulations have demonstrated that swimmer ray optics may be possible, so that viscosity lenses, prisms, and traps might be combined to organize swimmers to perform tasks. One possible application of swimmer ray optics is as an alternative to microfluidic lab-on-a-chip systems, where beams of microscopic swimmers could traffic molecular cargo across a chip. A fully autonomous system might be created, in which swimmers change shape based on their cargo and are routed accordingly through viscosity prisms, lenses, and traps.

Methods

We verify the theory and modeled swimmer ray optics through numerical simulation. In principle these simulations could be performed by explicitly modelling a phase separating liquid mixture with different viscosities for the different components, however, on the level of phenomena we are attempting to describe this would induce unnecessary computational burden. Instead, as a simplification, we use a position-dependent viscous damping term in the context of a standard Langevin dynamics approach. We solve the equation for the position of a particle in time \mathbf{r}

$$m \frac{d^2 \mathbf{r}}{dt^2} = -\gamma(\mathbf{r}) \frac{d\mathbf{r}}{dt} + \mathbf{F}(\mathbf{r}), \quad (17)$$

where m is the mass (in practice this value is low relative to the viscosity, setting a very short inertial timescale but one which nevertheless allows for greater numerical accuracy when iterating forward), $\gamma(\mathbf{r})$ is some spatially varying viscosity, and \mathbf{F} are the internal and swim forces.

The internal forces arise from the microscopic potentials we use in the simulation of which there are two types. Each bead has a steric repulsion, which gives an upper bound to the possible compressibility of the objects we consider. We use the Weeks-Chandler-Andersen potential for this purpose, given by

$$\phi_{\text{WCA}}(r) = \begin{cases} 4\epsilon \left(\left(\frac{\sigma}{r}\right)^{12} - \left(\frac{\sigma}{r}\right)^6 \right) + \epsilon, & r \leq 2^{1/6}\sigma \\ 0 & r > 2^{1/6}\sigma, \end{cases} \quad (18)$$

where σ is the hard sphere diameter $\sigma = 1$ and $\epsilon = 1$.

This is supplemented with the potentials necessary to give our objects structural rigidity, for which we use harmonic potentials

$$\phi_{\text{BOND}}(r) = \frac{1}{2}k(r - r_0)^2, \quad (19)$$

where r_0 is some rest length and k is an energy scale. For our simulations we first create an object of a given geometry, and then we add harmonic bonds between nearest neighbor particles where the rest length is taken as the original distance. In general, we set the energy scale k as large as possible in order to ensure structural rigidity of our objects.

The last element of the simulation is the swimming force exerted on the object. We take this force as acting uniformly on every particle. This force is given by

$$\mathbf{F}^{\text{swim}} = F_0(\cos \theta, \sin \theta), \quad (20)$$

where the angle θ is with respect to the internal axis (\mathbf{q}) of the object and the lab frame. In practice, we define the internal axes by taking a row of particles within the swimmer and averaging over the displacements between neighboring particles. The swimmer's orientation is then updated on each time step.

Simulation code is written in C++. Spatial dependence of viscosity is determined by the `spatial_viscosity` function in `mainShape.cpp`. Examples of how prism, ball lens, gradient lens and traps are defined within this function are in Section S1.5.

Acknowledgements

T.D.R. and P.W.K.R. were funded by the U.S. Department of Energy Award Number Department of Energy award DE-SC0020993. P.W.K.R. was additionally funded by the Office of Naval Research award N00014-18-1-2649. D.O. was partially supported by the U.S. Department of Energy, Office of Science, Office of Basic Energy Sciences, Award Number DE-SC-0010595 and partially through the Moore foundation. J.F.B. was funded by the National Science Foundation Grant 1803662.

Author contributions

T.D.R. and P.W.K.R. developed the core concept of the work. J.F.B. and T.D.R. worked on the analytical theory. D.O. built the simulation framework. T.D.R. ran and analyzed the simulations. All authors discussed results and wrote the manuscript.

References

1. Chowdhury, D., Schadschneider, A. & Nishinari, K. Physics of transport and traffic phenomena in biology: from molecular motors and cells to organisms. *Physics of Life Reviews* **2**, 318–352 (2005).
2. Lauga, E. & Powers, T. R. The hydrodynamics of swimming microorganisms. *Reports on Progress in Physics* **72**, 096601 (2009).
3. Chou, T., Mallick, K. & Zia, R. K. P. Non-equilibrium statistical mechanics: from a paradigmatic model to biological transport. *Reports on Progress in Physics* **74**, 116601 (2011).
4. Sánchez, S., Soler, L. & Katuri, J. Chemically Powered Micro- and Nanomotors. *Angewandte Chemie International Edition* **54**, 1414–1444 (2014).
5. Ebbens, S. Active colloids: Progress and challenges towards realising autonomous applications. *Current Opinion in Colloid & Interface Science* **21**, 14–23 (2016).
6. Peng, F., Tu, Y. & Wilson, D. A. Micro/nanomotors towards in vivo application: cell, tissue and biofluid. *Chemical Society Reviews* **46**, 5289–5310 (2017).
7. Li, J., de Ávila, B. E.-F., Gao, W., Zhang, L. & Wang, J. Micro/nanorobots for biomedicine: Delivery, surgery, sensing, and detoxification. *Science Robotics* **2**, eaam6431 (2017).
8. Luo, M., Feng, Y., Wang, T. & Guan, J. Micro-/Nanorobots at Work in Active Drug Delivery. *Advanced Functional Materials* **28**, 1706100 (2018).
9. Galajda, P., Keymer, J., Chaikin, P. & Austin, R. A Wall of Funnel Concentrates Swimming Bacteria. *Journal of Bacteriology* **189**, 8704–8707 (2007).
10. Wan, M. B., Reichhardt, C. J. O., Nussinov, Z. & Reichhardt, C. Rectification of Swimming Bacteria and Self-Driven Particle Systems by Arrays of Asymmetric Barriers. *Physical Review Letters* **101** (2008).

11. Stenhammar, J., Wittkowski, R., Marenduzzo, D. & Cates, M. E. Light-induced self-assembly of active rectification devices. *Science Advances* **2**, e1501850 (2016).
12. Frangipane, G. *et al.* Dynamic density shaping of photokinetic E. coli. *eLife* **7** (2018).
13. Arlt, J., Martinez, V. A., Dawson, A., Pilizota, T. & Poon, W. C. K. Painting with light-powered bacteria. *Nature Communications* **9** (2018).
14. Row, H. & Brady, J. F. Reverse osmotic effect in active matter. *Physical Review E* **101** (2020).
15. Chatterjee, P. & Goldenfeld, N. Field-theoretic model for chemotaxis in run and tumble particles. *Physical Review E* **103** (2021).
16. Cates, M. E. & Tailleur, J. Motility-Induced Phase Separation. *Annual Review of Condensed Matter Physics* **6**, 219–244 (2015).
17. Palacci, J., Sacanna, S., Steinberg, A. P., Pine, D. J. & Chaikin, P. M. Living crystals of light-activated colloidal surfers. *Science* **339**, 936–940 (2013).
18. Kantsler, V., Dunkel, J., Polin, M. & Goldstein, R. E. Ciliary contact interactions dominate surface scattering of swimming eukaryotes. *Proceedings of the National Academy of Sciences* **110**, 1187–1192 (2013).
19. Barnhart, E. L., Lee, K.-C., Keren, K., Mogilner, A. & Theriot, J. A. An Adhesion-Dependent Switch between Mechanisms That Determine Motile Cell Shape. *PLOS Biology* **9**, 1–19 (2011).
20. Coppola, S. & Kantsler, V. Green algae scatter off sharp viscosity gradients. *Scientific Reports* **11** (2021).
21. Datt, C. & Elfring, G. J. Active Particles in Viscosity Gradients. *Phys. Rev. Lett.* **123**, 158006 (15 2019).
22. Liebchen, B., Monderkamp, P., ten Hagen, B. & Löwen, H. Viscotaxis : Microswimmer Navigation in Viscosity Gradients. *Physical Review Letters* **120** (2018).
23. Ziebert, F. & Aranson, I. S. Computational approaches to substrate-based cell motility. *Computational Materials* **2**, 16019 (2016).
24. Nolte, D. D. *Snell's Law: The Fivefold Way in Gallileo Unbound: A Path Across Life the Universe and Everything* (Oxford University Press, New York, 2018), 1–10.
25. Liebchen, B. & Löwen, H. Optimal navigation strategies for active particles. *EPL (Europhysics Letters)* **127**, 34003 (2019).

Supplementary Information

S1 Simulation details

S1.1 Building shapes from particles

Here we describe how disks and rectangles are built up from particles and how the swimmer orientation is defined at each time step.

Swimmers are made up of discrete particles. The position of each particle is defined by each row of a csv file, where the x and y positions are the values in the first and second columns, respectfully. Bonds between particles is set by the interparticle distance of the initial configuration. Disk swimmers have a diameter of 29 particles. Rectangular swimmers have a length of 30 particles.

S1.2 Curve fitting and finding the critical angle

As discussed in the main text, the exact form of the drag coefficients depends on how the swimmer straddles the discontinuity. To generate the curves in Fig. 2a,b, and Fig. S3, we use a least-squares fit of the simulation data.

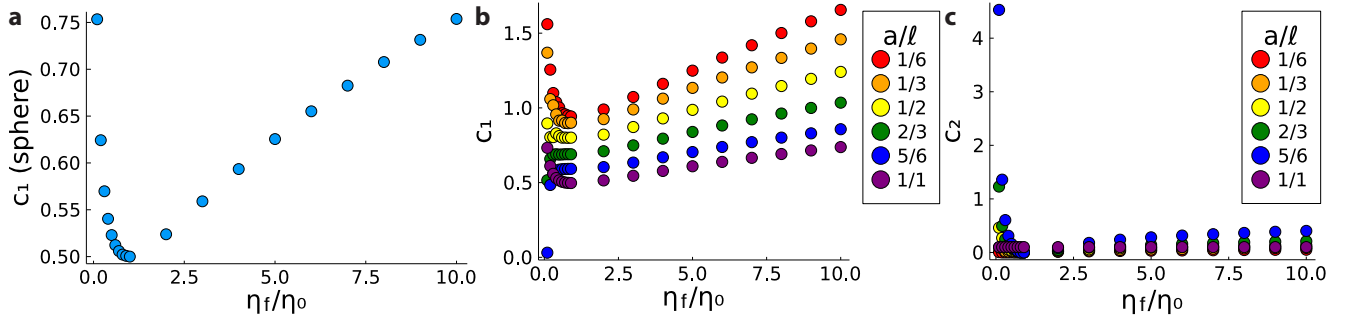


Figure S1: Fit parameters used to generate swimmer Snell's law curves. **a**, Fit parameter for spherical swimmer. **b,c**, Fit parameters for rectangular swimmer.

For the spherical swimmer we use

$$\sin \theta_f = \exp \left(-2c_1(\eta_f/\eta_0) \frac{\eta_f - \eta_0}{\eta_f + \eta_0} \right) \sin \theta_0, \quad (\text{S1})$$

where $c_1(\eta_f/\eta_0)$ is the free fit parameter that is determined for each viscosity ratio (Fig. S1a). We take the fit for $\sin \theta_f$ to avoid the boundary issue $\arcsin x \in \mathbb{R}$, $-1 \leq x \leq 1$. With the values for $c_1(\eta_f/\eta_0)$ in hand, we calculate the critical angle

$$\theta_{\text{crit}} = \arcsin \left(\exp \left(2c_1(\eta_f/\eta_0) \frac{\eta_f - \eta_0}{\eta_f + \eta_0} \right) \right). \quad (\text{S2})$$

For a rectangular swimmer we follow a similar procedure, but add a second fit parameter since the true Δx_{\perp} is now changed by the swimmer's rotation as it moves across the interface. We use

$$\sin \theta_f = \exp \left(-2 \frac{a}{\ell^2} (c_1(\eta_f/\eta_0, a/\ell)a + c_2(\eta_f/\eta_0, a/\ell)(\ell - a) \cos \theta_0) \frac{\eta_f - \eta_0}{\eta_f + \eta_0} \right) \sin \theta_0, \quad (\text{S3})$$

where $c_1(\eta_f/\eta_0, a/\ell)$ and $c_2(\eta_f/\eta_0, a/\ell)$ are fit parameters that are functions of viscosity ratios and the width-to-length ratio of the swimmer (Fig. S1b,c). We then find the rectangular swimmer's critical angle by numerically solving Eq. (S3) for $\sin \theta_{\text{crit}} = 1$.

S1.3 Further validation of Snell's law for swimmers

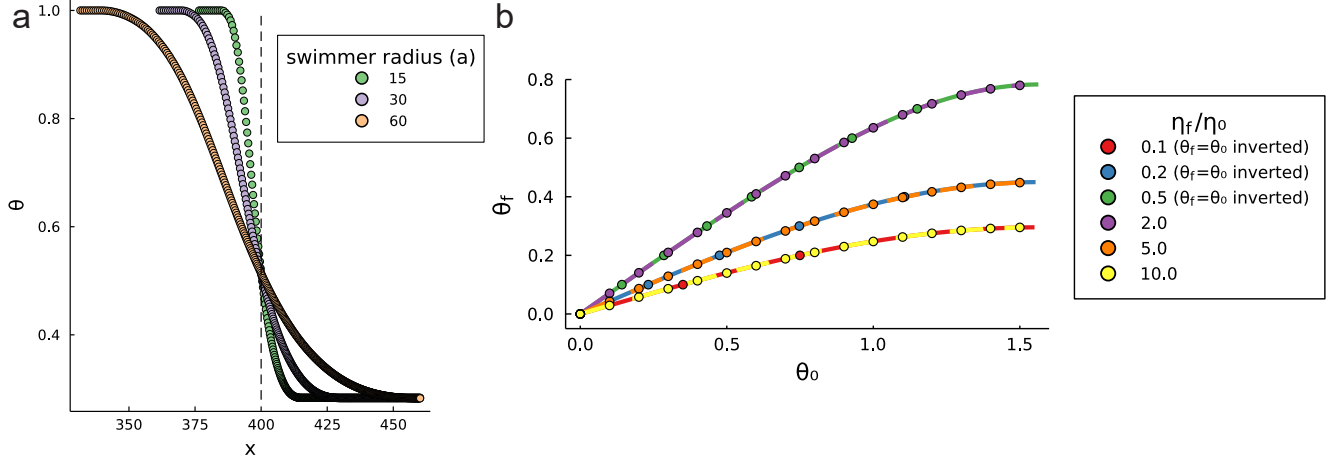


Figure S2: Further validation of Snell's law for spherical swimmer. **a**, Comparison of disk swimmers with different radii but the same incident angle ($\theta_0 = 1.0$) have the same final angle $\theta_f \approx 0.283$. The position of the viscosity discontinuity is indicated by the vertical dashed line. Spatial units are in particle length. **b**, Inversion of simulation data and curves for $\eta_f/\eta_0 < 1$ to demonstrate $\theta_f = \theta_0$ symmetry. Data points are simulation and curves are theory. Curves are dashed so that the overlap can be seen.

Eqs. (9) and (12) implies that the Snell's law is symmetric across the line $\theta_f = \theta_0$. We test this by taking a subset of simulation data and curves shown in Fig. 2a and inverting those corresponding to $\eta_f/\eta_0 < 1$ across the line $\theta_f = \theta_0$ Fig. S2b. The tight overlapping of the curves and data points to their mirror partner confirms this symmetry prediction.

S1.4 Wide rectangular swimmers

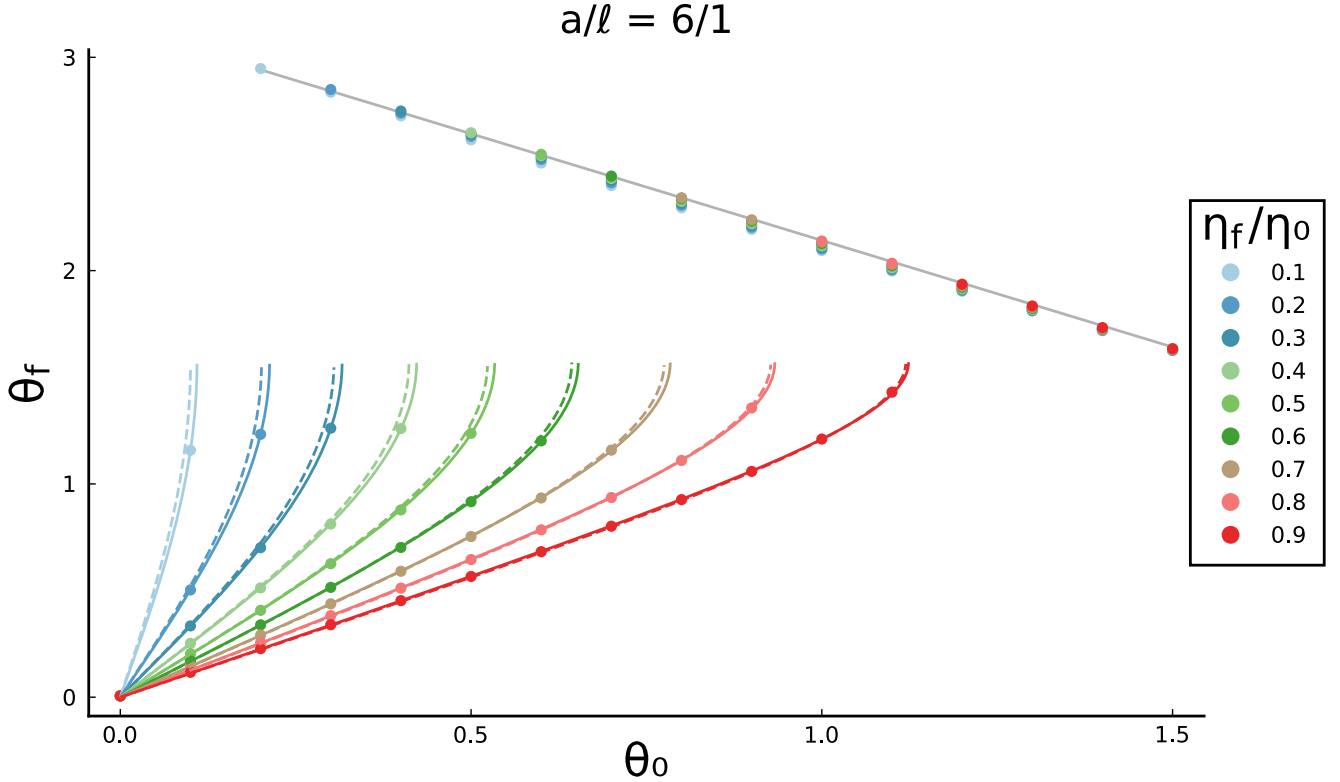


Figure S3: Refraction and reflection for a swimmer that is wide relative to its swim axis. The optical Snell's law for the equivalent speed ratios is plotted with dashed lines.

In Fig. 2c, we establish that refraction becomes less effective as a/ℓ becomes smaller. Conversely, as a/ℓ becomes larger, the effect of refraction increases. This remains true for swimmers with $a/\ell > 1$ (Fig. S3). In these simulations, the swimmer's width ($2a$) is 30 particles while the length (2ℓ) is shortened to 5 particles. For a wide swimmer, we must change the geometric scaling $\zeta_{rt}/\zeta_{rr} \sim \ell/a^2$, therefore changing Eq. (14) to $\alpha \sim -\frac{\ell}{a^2}(a + (\ell - a)\cos\theta_0)\frac{\Delta\eta}{\langle\eta\rangle}$. This change is accounted for when fitting the curves in Fig. S3.

We compare this result to the optical Snell's law for both the refraction curves in Fig. S3 and the critical angles in Fig. 2d using the equivalent speed ratios. We quantify the difference between refraction curves as

$$\% \text{ error} = \frac{\int \left| \theta_f^{\text{swim}}(\theta_0) - \theta_f^{\text{light}}(\theta_0) \right| d\theta_0}{\int \theta_f^{\text{light}}(\theta_0) d\theta_0}. \quad (\text{S4})$$

Based on the low errors (Table S1), we conjecture that in the limit that $a/\ell \rightarrow \infty$, the swimmer will converge to the optical Snell's law.

η_f/η_0	% error
0.1	12.63
0.2	6.57
0.3	4.33
0.4	2.85
0.5	1.83
0.6	1.12
0.7	0.81
0.8	0.57
0.9	0.61

Table S1: Comparison of wide swimmer curves to optical Snell's law.

S1.5 Defining the spatial dependence viscosity

The prism is an equilateral triangle where the length of each side is 10ℓ . For the top prism in Fig. 3a, the viscosity ratio is $\eta_{\text{prism}}/\eta_{\text{out}} = 2$, while the lower prism is $\eta_{\text{prism}}/\eta_{\text{out}} = 2/3$. The ball lens is created by making a disk-region of radius $\ell = 5$ with a viscosity ratio $\eta_{\text{b-lens}}/\eta_{\text{out}} = 8$. The gradient lens is a square with sides of length $\frac{40}{3}\ell$. The parabolic gradient is $\eta_{\text{g-lens}}/\eta_{\text{out}} = 2 \left(1 - \left(\frac{3(y/\ell - 20/3)}{40} \right)^2 \right)$. The trap is a disk of radius $r = 30\ell$ with viscosity $\eta_{\text{out}}/\eta_{\text{trap}} = 0.1$.

S1.6 Calculation of trapping probabilities

Trapping probabilities were determined by calculating the all possible incident angles that a swimmer could have for every point inside the trap. Trapping occurs when $\theta_0 > \theta_{\text{crit}}$ because a swimmer will continuously reflect to have the same incident angle across the circle. The average trapping probability is calculated by integrating the positional trapping probability and dividing it by the area of the trap.

S1.7 Optional thermal noise

Our simulation software can support the addition of random thermal forces $\boldsymbol{\xi}(t)$, which changes Eq. (17) for the position of a particle in time \mathbf{r} :

$$m \frac{d^2 \mathbf{r}}{dt^2} = -\gamma(\mathbf{r}) \frac{d\mathbf{r}}{dt} + \mathbf{F}(\mathbf{r}) + \boldsymbol{\xi}(t) \quad (\text{S5})$$

Thermal forces $\boldsymbol{\xi}(t)$ obeying white noise statistics,

$$\langle \boldsymbol{\xi}(t) \rangle = 0 \quad (\text{S6})$$

$$\langle \xi_i(t) \xi_j(t') \rangle = 2\delta_{i,j} \gamma(\mathbf{r}) k_b T \delta(t - t') \quad (\text{S7})$$